THE JOURNAL OF PHYSICAL CHEMISTRY C

Article

pubs.acs.org/JPCC

Nanoscale Optical and Mechanical Manipulation of Molecular Alignment in Metal−Molecule−Metal Structures

Katsuyoshi Ikeda,*[†,‡,§] Norihiro Fujimoto,[†,⊥] and Kohei Uosaki[†,§,∥]

[†]Division of Chemistry, Graduate School of Science, Hokkaido University, Sapporo, Hokkaido 060-0810, Japan

[‡]Japan Science and Technology Agency, PRESTO, 4-1-8 Honcho, Kawaguchi, Saitama 332-0012, Japan

[§]Global Research Center for Environment and Energy Based on Nanomaterials Science (GREEN), National Institute for Materials Science (NIMS), Tsukuba, Ibaraki 305-0044, Japan

[∥]International Center for Materials Nanoarchitectonics (WPI-MANA), National Institute for Materials Science (NIMS), Tsukuba, Ibaraki 305-0044, Japan

ABSTRACT: Equilibrium molecular orientations, monitored using surface enhanced Raman scattering, are controlled by both optical and mechanical means in metal−molecule−metal nanogap structures, formed on an atomically planar Au(111) surface. The spatially confined optical near-fields exert a torque on the molecules in the nanogaps and align the molecular orientations along the field vector. The mechanical compression from the metal nanogaps not only disturbs the molecular alignments but also perturbs the electronic structures at metal−molecule interfaces. The implications of such interactions are discussed with respect to control and detection of local electronic properties in molecular nanodevices.

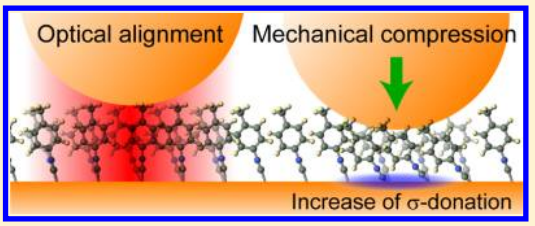

1. INTRODUCTION

Characterizing molecular responses at the nanoscale is vitally important in various fields with respect to both fundamental research and applications. In particular, investigation of photon−molecule interactions at the nanoscale has been a rapidly growing scientific activity during the past decade.[1−4] The spatial focusing of optical waves is usually governed by the diffraction limit, so that the nanometric localization of optical fields must be mediated by excitation of polaritons, such as surface plasmon polaritons on a metal nanostructure.[5−7] Such field localization causes enhancement of the photon−molecule interaction efficiency in the vicinity of the metal nanostructures. Surface enhanced Raman scattering (SERS) spectroscopy is one of the most successful applications of the local enhancement effect.[8,9] The extremely large enhancement has led to the possibility of single molecule spectroscopy being discussed in the SERS community.[10−12] Photochemical processes such as photoenergy conversion can also benefit from the local enhancement effect. The enhancement effects for optical and photochemical efficiency are considered to be the interplay of energy between photons and molecules via plasmons, which is now becoming controllable due to the efforts of many researchers.[13−18]

The momentum exchange effect between photons and molecules is also of significant interest in the optics community.[19−22] The optical manipulation of molecules is an especially fascinating phenomena in terms of both fundamental questions and practical applications. For far-field radiation, the optical manipulation of molecules, such as polarization-induced alignment of molecules, has been studied in detail for both condensed and gas phases.[23,24] However, near-field manipulation of molecules is still unclear, despite a number of theoretical and experimental attempts.[25−28] At the nanoscale, the orientational control of molecules bound to a metal electrode surface is of potential importance for molecular electronics.[29,30] If molecular alignment is controlled in metal−molecule−metal junctions, then electronic conductance could be switched, which would lead to the development of molecular logic, memory, and sensing.

To manipulate molecules optically at the nanoscale, there are two issues that require consideration. First, spatially and orientationally inhomogeneous optical near-fields must be carefully managed through control of the size and shape of the metal nanostructures.[5−7] In the past decade, this has improved from significant advancements in nanofabrication technology.[17,31−33] Second, molecular orientations must be well-defined on the metal substrate in the equilibrium condition. This factor is critically dependent on metal−molecule interactions;[34−38] therefore, the metal surface must be managed uniformly at the atomic scale. Thus, both the nanometric shapes and atomic surface features of the metal nanostructures must be controlled simultaneously, which is practically difficult even at the current level of nanotechnology.

For molecular manipulation, mechanical control of molecules is also quite of interest as well as optical control. It is vitally important to fields such as microelectromechanical systems (MEMS) or molecular electronic devices, where the behavior of nanoscale metal−molecule contacts can determine the system

Received: April 14, 2014
Revised: June 17, 2014

   dx.doi.org/10.1021/jp5036426 | J. Phys. Chem. C XXXX, XXX, XXX−XXX

reliability, lifetime, and performance. However, characterization of the mechanical response of molecules at the nanoscale is technically challenging due to the limited detection techniques. The use of optical near-fields appears to be a good solution to monitor the dynamical motion of molecules at the nanoscale. The atomic force microscopy (AFM) tip-induced deformation of carbon nanotubes has been monitored using tip-enhanced Raman spectroscopy (TERS), which may lead to local modification of the electronic properties of nanomaterials.[39] Fishing for a molecule using a scanning tunneling microscopy (STM) tip has also been investigated using the TERS technique.[40]

Recently, we have demonstrated that a sphere−plane type metal nanogap structure is suitable for simultaneous control of both the nanometric shapes and atomic surface features in plasmonic systems.[37,41−44] In this structure, a metal nanosphere is almost in contact with a metal plane having an atomically defined smooth surface. This is achieved practically by the deposition of metal nanoparticles on top of a chemically modified single crystalline metal substrate. Thus, molecules located in the nanogap have two roles when SERS is measured in this system: spacer and Raman scatterer. The plasmon resonance features of the nanogap structures are well characterized by the spacer thickness. Due to the strong field localization within the nanogaps, only molecules within the gaps can be selectively monitored using SERS.[45−47] Moreover, the present "freestanding" metal nanogaps with molecular spacers are expected to be rather flexible, unlike conventional metal nanogap systems formed on a dielectric substrate; a molecular spacer may be compressed by the application of pressure. These are significant advantages for the study of both optical and mechanical responses for metal−molecule systems in nanogaps.

In this work, we demonstrate that the molecular orientations in metal−molecule−metal structures can be controlled by optical near-fields. SERS spectra clearly show that the local fields exert a torque on the molecular dipoles; the molecular equilibrium configuration becomes more parallel to the local fields as the incident power increases. In addition, the mechanical compression of molecular monolayers is observed in situ in the metal nanogaps and their behavior is characterized with respect to the structural and electronic perturbations at the metal−molecule interfaces.

2. METHODS

Figure 1a shows a schematic illustration of the sphere−plane type metal nanogap structure employed in this study. To manage the atomic surface features of the metal plane, a Au single crystalline microbead with (111)-facets was prepared by the Clavilier method.[48] The atomic flatness of the obtained surface was examined using AFM. The microbead was then immersed into a tetrahydrofuran (THF) solution containing 10 mM 4-methylphenyl-isocyanide (MPI; Oakwood Products, Inc.) under an argon atmosphere to produce well-organized self-assembled monolayers (SAMs) on the Au(111) surface. This molecule binds to the substrate with a lone electron pair on the carbon atom of the NC group and forms an edge-on configuration.[41,49] Finally, Au nanoparticles (Au NPs) with ca. 20 nm diameters were physisorbed on top of the SAMs by immersion of the chemically modified substrate into a colloidal solution of citrate-reduced Au NPs. As shown in Figure 1b, the negatively charged Au NPs were spatially isolated from each other on the SAM, indicating that the interparticle plasmon

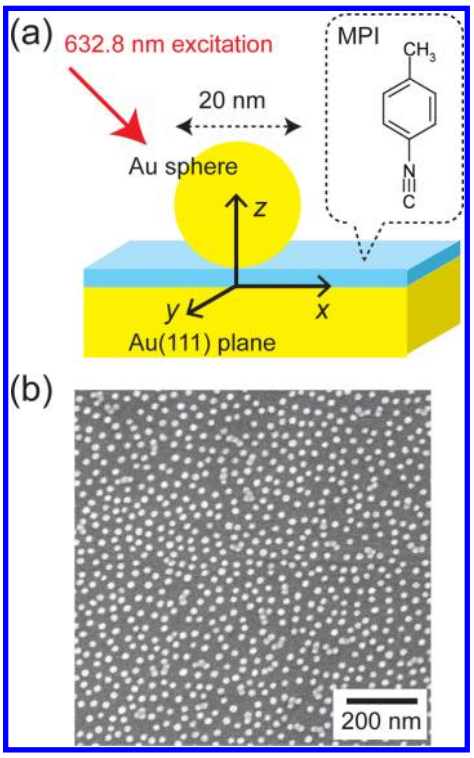

Figure 1. (a) Schematic illustration of a sphere−plane system for gap-mode plasmon excitation at well-defined metal−molecular interfaces and the molecular structure of MPI. The laboratory frame is also shown in the figure; the *z*-axis is normal to the plane, and the Au substrate surface is along the *xy*-plane. (b) SEM image of Au NPs with a size of 20 nm adsorbed on the MPI-modified Au(111) surface.

coupling is insignificant in the present system.[46,47] We have previously confirmed that the chemically bonded NC−Au(111) interface remains intact in the presence of Au NPs; transfer of isocyanides from the substrate surface to the Au NP surfaces was negligible during the SERS experiments.[37,42]

The 632.8 nm radiation from a He−Ne laser was utilized to excite localized plasmon modes at the Au NPs−MPI−Au(111) nanogaps. SERS signals from MPI SAMs within the nanogaps were selectively monitored on the Au(111) facet using an in-house-built inverted microscope with an objective lens (40×, 0.6 N.A.). Electrochemical SERS experiments were conducted under potential control of the Au(111) substrate using a three-electrode cell. The thickness of the MPI SAM and the reflectance of the Au NPs−MPI−Au(111) surface were measured using a spectroellipsometer.

The local field distribution around an Au NP above the Au plane was calculated for the 632.8 nm excitation using the finite-difference time-domain (FDTD) method (FDTD Solutions, Lumerical Solutions, Inc.). Cross sections of an Au NP above the Au plane were calculated as a function of wavelength under a static field approximation by taking into account multipole interactions between the Au NP and Au plane.[50,51] Then, the simulated reflectance spectrum was obtained by considering the surface density of Au NPs shown in Figure 1b. In the calculations, the thickness of MPI SAMs was fixed at 0.4 nm, which was determined experimentally. Raman active vibration modes of MPI molecules were calculated using Gaussian 09, revision A02, at the B3PW91 level of theory with the LanL2DZ basis set for the Au atom and 6-31G** basis sets for other atoms.

dx.doi.org/10.1021/jp5036426 | J. Phys. Chem. C XXXX, XXX, XXX−XXX

3. RESULTS AND DISCUSSION

3.1. Local Field Enhancement in Sphere−Plane Nanogap Structures. According to the electromagnetic theory,[46,47] the optical near-fields in this system are well characterized by the sphere−plane distance. This can be understood by a simple picture of the electromagnetic interaction between an induced dipole on the sphere and a mirror dipole in the substrate, although higher-order contributions must also be taken into consideration. The sphere−plane distance in this case is nearly equal to the SAM thickness, as shown in Figure 1a. Since evaluation of the local field enhancement is critical to studying optical near-field manipulation of molecules in the nanogaps, the plasmon resonance characteristic of the sphere−plane system was first examined by both theoretical and experimental means.

Figure 2a shows a comparison between the theoretical calculation and experimental measurement of reflectance spectra of the Au NPs−MPI−Au(111) surface under the p-polarization configuration. In the calculated spectrum, the largest peak at 590 nm can be assigned to the dipolar plasmon mode and the shoulder peak at 530 nm to the higher-order multipole plasmon mode; these so-called gap-modes are built as a result of the strong hybridization between the induced dipoles on Au NPs and the mirror dipoles in Au(111). These spectral features are found in the experimentally obtained spectrum, although the peak widths are much broader. Since the interparticle plasmon coupling is not considered in the calculation, this similarity indicates that the sphere−plane nanogap structures on Au(111) are well isolated from each other. Therefore, the electromagnetic fields are substantially enhanced only in the gaps between the Au NPs and Au substrate.

The local enhancement of the optical intensity around a nanogap, $|E_{loc}/E_0|^2$, was simulated for p-polarized 632.8 nm excitation with an incident angle of 45°. Here, E_{loc} and E_0 denote the local field and the incident field, respectively. The simulated local field vector is decomposed to the z-component in Figure 2b and the x-component in Figure 2c. As expected from the theory, the electric fields are highly localized in the gap between the Au NP and Au substrate, and the field vector within the gap is dominantly oriented normal to the atomically planar substrate. Therefore, when the gap-mode plasmons are excited, MPI molecules located in the gaps are exposed to the homogeneous and enhanced electric fields. Since the enhancement factor, $|E_{loc}/E_0|^2$, is expected to be more than 10^3 in the nanogap, optically induced orientational change of MPI molecules is likely to take place only in the nanogaps.

It is widely accepted that the SERS enhancement is ascribed to two different mechanisms.[52,53] The main contribution is the local field enhancement due to plasmonic resonances, i.e., the electromagnetic (EM) effect.[54,55] The other enhancement mechanism is related to electronic resonances at metal−molecule interfaces, i.e., the charge transfer (CT) effect.[56] The EM contribution to the SERS enhancement is expressed as the fourth power of the field enhancement, $|E_{loc}/E_0|^4$, when the Stokes-shifted frequencies are close to the excitation frequency. According to Figure 2b, the EM enhancement expected in the nanogaps is more than 10^6, suggesting that information regarding the field-induced change of MPI molecules in the nanogaps can be selectively monitored using SERS.

3.2. Raman Bands of MPI Molecules. In SERS spectra, the EM effect can enhance only totally symmetric vibrations,

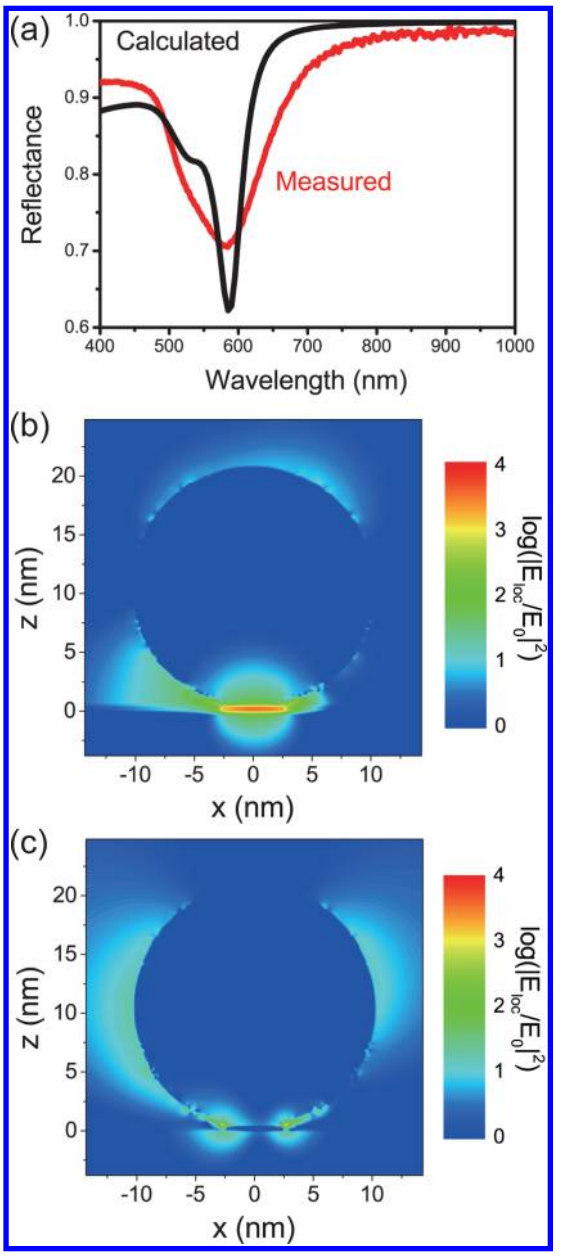

Figure 2. (a) Reflectance spectra of Au NPs−MPI−Au(111) measured and calculated with p-polarization conditions. (b) Spatial distribution of the z-component of the simulated local field vector, E_{loc}, around the Au sphere on the thin layer-covered Au plane, calculated for p-polarized 632.8 nm excitation with an angle of 45°. (c) Spatial distribution of x-components of the field vector calculated for the same condition.

while the Herzberg−Teller type CT is effective for the enhancement of nontotally symmetric modes.[52] Therefore, the orientational change of molecules will appear as a variation of relative intensities between totally and nontotally symmetric modes according to the surface selection rules. The CT contribution in SERS spectra can be distinguished by changing the Fermi level of the metal substrate under electrochemical potential control. Such information should be helpful to discuss the orientational change of molecules.

Figure 3a presents the electrochemical potential dependent SERS spectra of Au NPs−MPI−Au(111) in 0.1 M $NaClO_4$ aqueous solution, measured under 0.02 mW excitation. Assignments of the observed Raman bands are indicated in

dx.doi.org/10.1021/jp5036426 | J. Phys. Chem. C XXXX, XXX, XXX−XXX

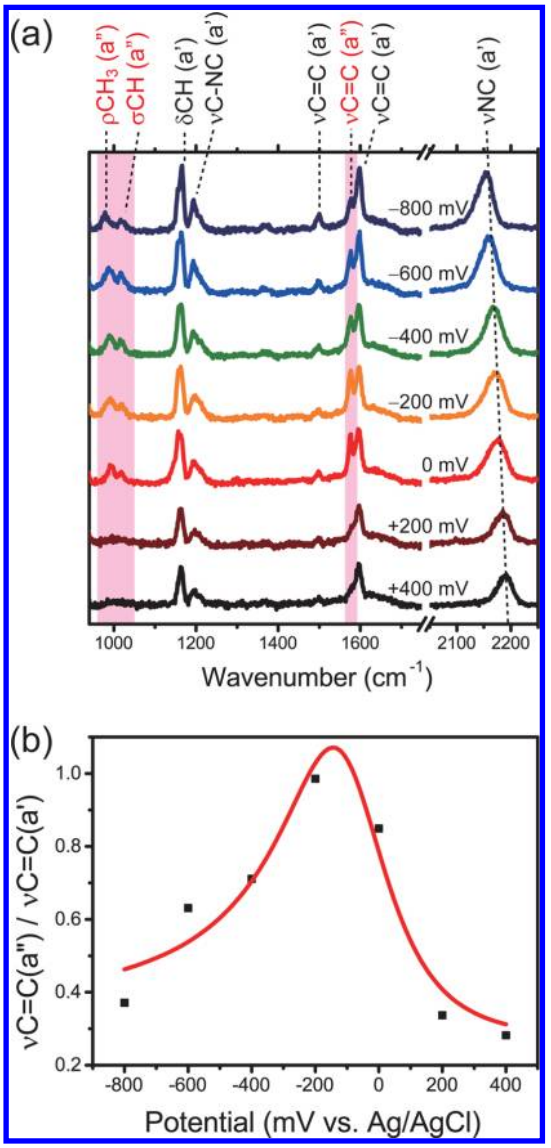

Figure 3. (a) Electrochemical potential-dependent SERS spectra of Au NPs−MPI−Au(111) in 0.1 M $NaClO_4$ solution. The potential of the Au(111) electrode was swept between +400 and −800 mV vs Ag/AgCl. (b) Asymmetric potential profile of the νC═C(a″) intensity relative to the νC═C(a′) intensity. Curve fitting was conducted using Fano resonance theory, which includes coupling of the molecular vibrational levels with the continuum of levels in the conduction band in the metal.[57] a′ and a″ denote totally symmetric and nontotally symmetric vibrations, respectively.

the figure. According to the C_s symmetry of MPI molecules, the vibration modes are classified as totally symmetric a′ and nontotally symmetric a″ species. During the potential sweep between +400 and −800 mV vs Ag/AgCl, two types of spectral variations were observed. One of the significant changes is a frequency shift of the NC stretching mode, i.e., νNC(a′); the peak position is red-shifted on the cathodic scan. The shift of the νNC frequency is almost proportional to the electrochemical potential with a gradient of 0.032 cm^{-1}/mV. Similar peak shifts have been reported for various isocyanide molecules in IR and conventional SERS experiments.[57,58] The other significant change in Figure 3a is the potential-dependent intensity of the peaks at 987, 1016, and 1577 cm^{-1}, which are assigned as ρCH_3, σCH, and νC═C with the a″ symmetry, respectively. For the other peaks having a′ symmetry, no considerable change of intensity was observed in this potential region, which suggests that the molecular orientation is not significantly affected by the applied potential. During the potential scan toward the negative direction, the intensity of these three a″ modes rapidly increased and then gradually decreased with the maximum at around −200 mV, as shown in Figure 3b. Such an asymmetric potential profile is recognized as the characteristic feature of CT enhancement.[56,59] Hereinafter, these potential dependent a″ peaks are referred to as CT-induced bands, while the other a′ peaks are ascribed as EM-induced bands.

Figure 4 shows a rough energy level diagram of the MPI−Au interface. For MPI molecular orbitals, the energy levels and wave functions in a vacuum were calculated using the DFT method. According to the d-band theory,[60,61] these molecular orbitals first couple with the sp-electrons of Au(111), leading to the broadening and downshifts in energy. These broadened bands further hybridize with the d-band to split into corresponding bonding and antibonding states. Among these hybridized states, the d-σ antibonding and d-π* bonding orbitals dominantly contribute to the formation of NC−Au bonding through σ donation and π back-donation. The degrees of these electron donations can be tuned electrochemically; the upshift of the electrochemical potential causes a decrease of σ-donation and an increase of π back-donation, as shown in the left bottom panel of the figure.[41,49] Since the σ- and π*-orbitals of MPI are antibonding with respect to the NC bond, such potential tuning leads to a decrease in the νNC frequency.[57,58]

The electrochemical potential tuning may also change the degree of the CT resonance, as illustrated in the right bottom panel of Figure 4. In the present case, the molecule-to-metal CT is expected to be induced at the MPI−Au(111) interface. The CT direction can be determined by fitting of the experimental data in Figure 3b using the Fano resonance theory.[59] The asymmetry parameter q in Fano notation was estimated to be −4.8; the negative q corresponds to molecule-to-metal CT because this value is closely related to phase difference in the interference between the metal continuum states and a discrete molecular state. During the electrochemical potential sweep, the CT-induced band intensities become maximum at around −200 mV vs Ag/AgCl, at which the energy difference between the Fermi level of Au and the ground state of MPI is equal to the excitation energy of 1.96 eV (632.8 nm). Under such resonance conditions, the CT transition can gain intensity through intensity borrowing from an allowed optical transition of MPI molecules. According to the DFT calculation, the allowed transition takes place from HOMO/HOMO−1 to LUMO+1/LUMO ($^1A' \rightarrow {}^1A''$). Since the CT dipole from MPI to Au is of A′ symmetry, the vibronic coupling between the excited A″ state and the metal states can induce the appearance of a″ modes according to the surface selection rule ($A' \times A'' = a''$).

3.3. Optical Near-Field Manipulation of MPI Molecules. Figure 5a shows excitation power dependent SERS spectra of Au NPs−MPI−Au(111) under ambient conditions without electrochemical potential control. Each spectrum is normalized with respect to the νC═C(a′) because the intensity of this EM-induced band was almost proportional to the excitation power. The most interesting aspect in this figure is the intensity variation of the CT-induced a″ bands relative to the EM-induced a′ bands. This change was reversible and reproducible, so that the possibility of photochemical changes

dx.doi.org/10.1021/jp5036426 | J. Phys. Chem. C XXXX, XXX, XXX−XXX

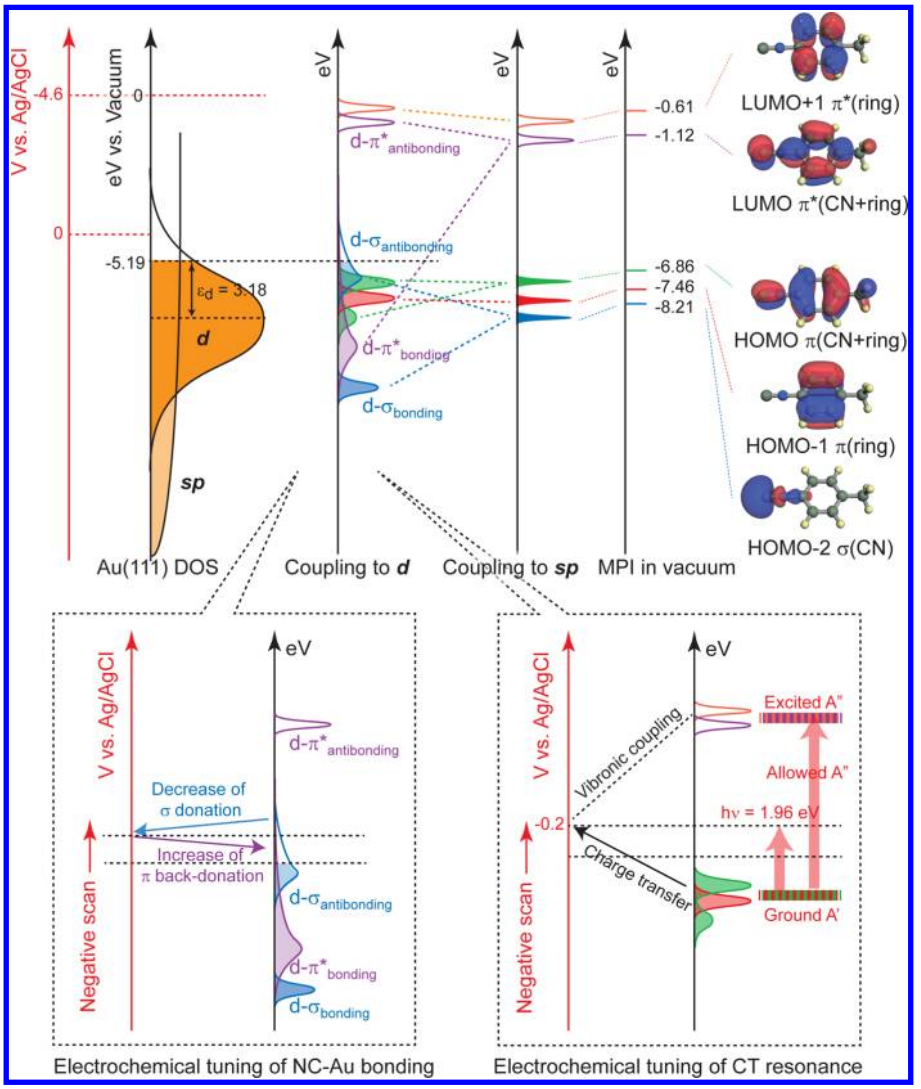

Figure 4. A rough energy levels diagram of the MPI−Au interface, on the basis of the d-band theory, with density of states of Au(111) and DFT calculated molecular orbitals of MPI in a vacuum. The hybridized states are expressed by broadening and downshifts of the molecular orbitals due to coupling to sp-electrons of Au and by splitting to bonding and antibonding orbitals due to coupling to d-electrons of Au. The left bottom panel shows electrochemical tuning of NC−Au bonding through variation of σ donation and π back-donation. The right bottom panel explains electrochemical tuning of CT resonance due to variation of the energy difference between the Fermi level of Au and the molecular ground state.

of the molecules under intense excitation can be excluded. In contrast with the electrochemical SERS shown in Figure 3a, this intensity change was not accompanied by a frequency shift of the νNC. This result strongly suggests that any electronic change at the interface was negligible under the present laser excitation conditions, because variation of the energy level difference would lead to both the intensity change of the CT-induced bands and the frequency shift of the νNC band simultaneously, as already explained in Figure 4. Therefore, the invariance of the νNC frequency strongly raises the possibility of the optically induced orientational change of MPIs, which will be further discussed later. The excitation power dependence of the band intensities is summarized in Figure 5b. When the excitation power increased, the CT-induced νC═C(a″) band (as well as the other CT-induced bands) was significantly increased relative to the EM-induced νC═C(a′) band. In addition, the EM-induced δCH(a′) band slightly increased relative to the νC═C(a′) band with an increase in the excitation power. The νC—CH_3(a′) band also seems to be larger with increasing excitation power. Incidentally, these power-dependent spectral variations were not clearly observed with conventional SERS measurements on a roughened Au substrate.

Here, it should be again noted that the CT transition moment is perpendicular to the metal substrate.[56,58] Hence, the nontotally symmetric CT-induced band intensities are critically sensitive to molecular orientations relative to the EM-induced totally symmetric band intensities. For the present three CT-induced a″ bands, the intensity becomes maximized when the MPI molecule is standing up perpendicular to the atomically planar Au(111) substrate. According to our previous study using vibrational sum-frequency generation spectroscopy, the equilibrium configuration of MPIs is tilted with an average angle of 13°.[62] Therefore, it is assumed that the orientation of MPIs in the nanogaps is also tilted in the absence of electromagnetic fields. If the molecular dipole and the local near-field have different orientations, then the fields can exert a torque on the molecules.[26,27] The local field vector in the nanogaps is oriented along the z-axis as a result of the plasmon hybridization between Au NP and Au(111).[45−47] Therefore, it

dx.doi.org/10.1021/jp5036426 | J. Phys. Chem. C XXXX, XXX, XXX−XXX

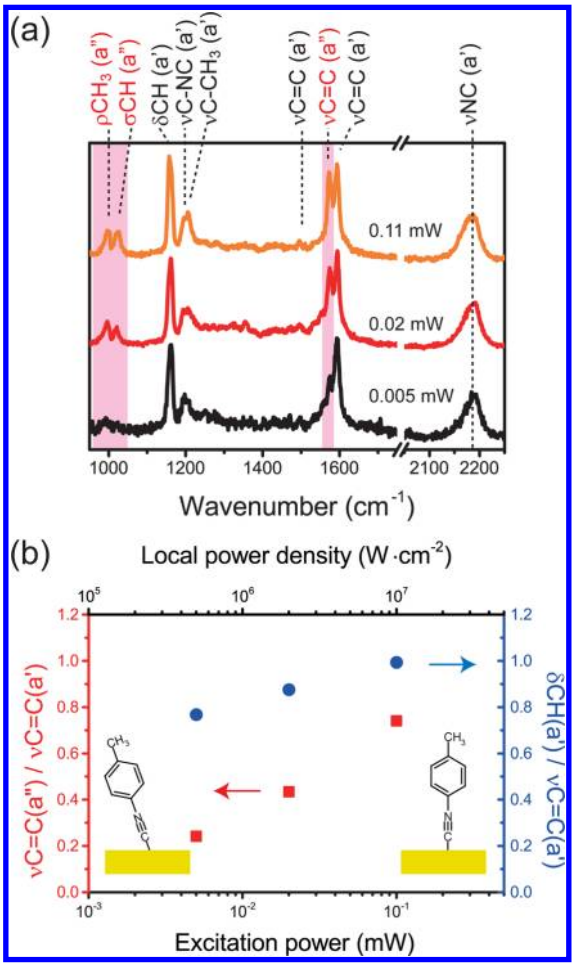

Figure 5. (a) Excitation power-dependent SERS spectra of Au NPs−MPI−Au(111) under ambient conditions. (b) Excitation power dependence of the νC═C(a″) and δCH(a′) band intensities relative to the νC═C(a′) band intensity. The lower axis indicates the experimentally measured excitation power at the focus spot. The upper axis indicates the local power density at a nanogap, which is expected from the FDTD result shown in Figure 2b.

is reasonable that the equilibrium configuration of MPI becomes more vertical under intense excitation. The synchronous change of the EM-induced δCH(a′) and νC—CH_3(a′) to the CT-induced a″ bands is also well explained by assuming the field-induced alignment of MPIs. The change in the νC═C band is rather small compared with those in the δCH and νC—CH_3 bands due to the difference of the polarizability tensor components among these modes.

The maximum excitation power employed in the present experiment corresponds to 1×10^4 W cm^{-2}. This is not generally sufficient to induce any observable angular motion of molecules.[26,27] However, by considering the field enhancement effect shown in Figure 2b, the intensity in the nanogaps can reach more than 1×10^7 W cm^{-2} (see upper axis in Figure 5b). This is probably comparable to the intensity that can induce detectable variations of the MPI configuration.

3.4. Mechanical Manipulation of MPI Molecules in Metal Nanogaps. The equilibrium molecular configuration can also be changed by mechanical control of the metal−molecule−metal structure. The gap distance in the freestanding sphere−plane system is expected to be reduced by the application of mechanical pressure to the Au NPs. In the present experiment, the application of pressure was conducted using a glass slip equipped with a piezo-electric z-stage. Note that the use of the atomically planar Au(111) substrate enables such mechanical deformation of the SERS-active hotspots to be conducted. Figure 6 shows SERS spectra of Au NPs−MPI−

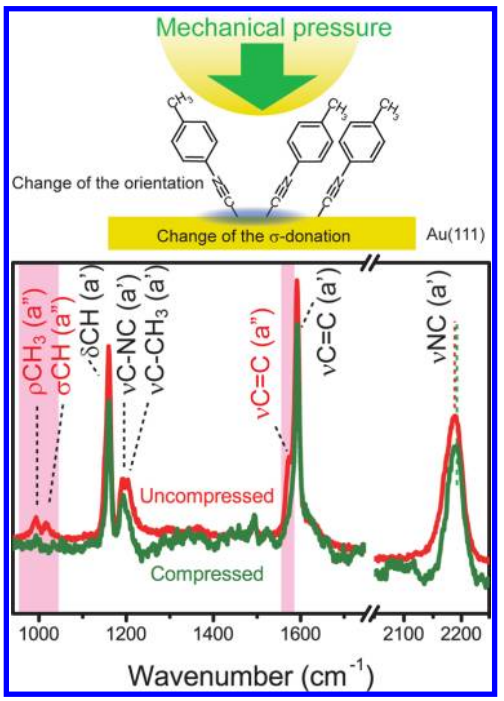

Figure 6. SERS spectra of Au NPs−MPI−Au(111) measured with and without mechanical compression. The upper panel shows a schematic of the mechanical deformation within the nanogap.

Au(111) with and without the mechanical compression, measured with the 0.005 mW excitation. The increase in the spectral noise under the compression is due to the fluorescence from the glass substrate. Only the bands that exhibited the power-dependent change in the relative intensities, i.e., $\rho$$CH_3$(a″), σCH(a″), νC═C(a″), δCH(a′), and νC—CH_3(a′), were significantly responsive to the pressure application. It is thus assumed that the orientation of MPIs in the gaps was changed from the equilibrium configuration by mechanical compression, leading to the decrease of the CT contribution. Moreover, the frequency of the νNC peak was slightly blue-shifted under pressure application, which is quite different from the optical alignment of MPIs shown in Figure 5. This characteristic implies an increase of σ-donation from the NC group to the Au substrate. Since the applied load is too weak to induce any shift in the Fermi level of Au, the increase of the electron donation must be due to compression of the NC−Au bond;[57,58] the shortening of the NC triple bond is rather difficult due to Pauli repulsion. If we assume that the NC bond length is invariant under pressure application, the observed peak shift of ca. 5 cm^{-1} approximately corresponds to a shortening of the NC−Au bond length by 0.02 Å (nearly 1% of the original bond length), according to the DFT calculation. This mechanically induced electron donation is related to the increase of the energy splitting between the bonding and antibonding d-σ orbitals in the Au−MPI hybridized electronic states. Such a change in the interfacial electronic structure should lead to a variation of the electronic conductance at the metal−molecule junction. This mechano-

dx.doi.org/10.1021/jp5036426 | J. Phys. Chem. C XXXX, XXX, XXX−XXX

electric coupling at metal−molecule interfaces may provide a noble possibility for development of molecular nanodevices.

In the meantime, it is difficult to estimate the practically applied load onto each Au NP, because the number of Au NPs within the microscope focus was around 200. When TERS is employed, the pressure application may be better controlled, although the optical alignment effect or local heating would not be avoided, due to the intense excitation required to obtain analyzable spectra from a sole hot spot.

4. SUMMARY

We have observed SERS spectra of isocyanide monolayers in metal nanogaps under various external stimuli, such as electrochemical potential, optical near-fields, and mechanical compression. Although SERS spectroscopy is a powerful tool to investigate a small number of molecules at the nanoscale, it often suffers from inhomogeneous surface atomic features. In the present experiment, the formation of nanogaps on the single crystalline Au(111) substrate enabled us to obtain highly reproducible SERS spectra and to investigate dynamical motion of molecules.

Plasmonically confined optical near-fields induced angular motions to the molecules in the metal nanogaps. Optical control of molecular orientation in metal−molecule−metal junctions should lead to the possibility of optical switching of various physical properties such as conductance at the nanoscale, which will be indispensable for advancements in molecular devices. Mechanical compression of the metal nanogaps induced distortional change of the molecular alignment. Moreover, the frequency shift of the NC anchor group was quite sensitive to pressure application, which could be exploited to detect local stress in nanodevices. This shift is closely related to the variation of σ-donation; therefore, interfacial electronic coupling may also be affected by mechanical compression, which may open up a novel avenue to tune electron transport at metal−molecule interfaces.

AUTHOR INFORMATION

Corresponding Author

*Phone: +81-11-706-2708. E-mail: kikeda@pchem.sci.hokudai.ac.jp.

Present Address

[⊥]NTT Energy and Environment Systems Laboratories, Nippon Telegraph and Telephone Co., Tokyo 180-8585, Japan.

Notes

The authors declare no competing financial interest.

ACKNOWLEDGMENTS

This research was supported in part by a Grant-in-Aid for Young Scientists (A) (No. 24681018) and a Grant-in-Aid for Exploratory Research (No. 24651126) from the Japan Society for the Promotion of Science (JSPS), World Premier International Research Center (WPI) Initiative on Materials Nanoarchitechtonics, and the Program for Development of Environmental Technology using Nanotechnology of the Ministry of Education, Culture, Sports, Science and Technology (MEXT), Japan.

REFERENCES

(1) Hutchison, J. A.; Schwartz, T.; Genet, C.; Devaux, E.; Ebbesen, T. W. Modifying Chemical Landscapes by Coupling to Vacuum Fields. *Angew. Chem., Int. Ed.* **2012**, *51*, 1592−1596.

(2) Schlather, A. E.; Large, N.; Urban, A. S.; Nordlander, P.; Halas, N. J. Near-Field Mediated Plexcitonic Coupling and Giant Rabi Splitting in Individual Metallic Dimers. *Nano Lett.* **2013**, *13*, 3281−3286.

(3) Koppens, F. H. L.; Chang, D. E.; García de Abajo, F. J. Graphene Plasmonics: A Platform for Strong Light-Matter Interactions. *Nano Lett.* **2011**, *11*, 3370−3377.

(4) Aikens, M. A.; Madison, L. R.; Schatz, G. C. Raman Spectroscopy: The Effect of Field Gradient on SERS. *Nat. Photonics* **2013**, *7*, 508−510.

(5) Bharadwaj, P.; Deutsch, B.; Novotny, L. Optical Antennas. *Adv. Opt. Photonics* **2009**, *1*, 438−483.

(6) Barnes, W. L.; Dereux, A.; Ebbesen, T. W. Surface Plasmon Subwavelength Optics. *Nature* **2003**, *424*, 824−830.

(7) Maksymov, I. S.; Staude, I.; Miroshnichenko, A. E.; Kivshar, Y. S. Optical Yagi-Uda Nanoantennas. *Nanophotonics* **2012**, *1*, 65−81.

(8) Fleishmann, M.; Hendra, P. J.; McQuillan, A. J. Raman Spectra of Pyridine Adsorbed at a Silver Electrode. *Chem. Phys. Lett.* **1974**, *26*, 163−166.

(9) Jeanmaire, D. L.; Van Duyne, R. P. Surface Raman Spectroelectrochemistry: Part I. Heterocyclic, Aromatic, and Aliphatic Amines Adsorbed on the Anodized Silver Electrode. *J. Electroanal. Chem.* **1977**, *84*, 1−20.

(10) Kneipp, K.; Wang, Y.; Kneipp, H.; Perelman, L. T.; Itzkan, I.; Dasari, R. R.; Feld, M. S. Single Molecule Detection Using Surface-Enhanced Raman Scattering (SERS). *Phys. Rev. Lett.* **1997**, *78*, 1667−1669.

(11) Nie, S.; Emory, S. R. Probing Single Molecules and Single Nanoparticles by Surface-Enhanced Raman Scattering. *Science* **1997**, *275*, 1102−1106.

(12) Zhang, R.; Zhan, Y.; Dong, D. C.; Znag, C.; Chen, L. G.; Zhang, L.; Liao, Y.; Aizpurua, J.; Luo, Y.; Yang, J. L.; et al. Chemical Mapping of a Single Molecule by Plasmon-Enhanced Raman Scattering. *Nature* **2013**, *498*, 82−86.

(13) Akiyama, T.; Nakada, M.; Terasaki, N.; Yamada, S. Photocurrent Enhancement in a Porphyrin-Gold Nanoparticle Nanostructure Assisted by Localized Plasmon Excitation. *Chem. Commun.* **2006**, *4*, 395−397.

(14) Ikeda, K.; Takahashi, K.; Masuda, T.; Uosaki, K. Plasmonic Enhancement of Photoinduced Uphill Electron Transfer in a Molecular Monolayer System. *Angew. Chem., Int. Ed.* **2011**, *50*, 1280−1284.

(15) Ikeda, K.; Takahashi, K.; Masuda, T.; Kobori, H.; Kanehara, M.; Teranishi, T.; Uosaki, K. Structural Tuning of Optical Antenna Properties for Plasmonic Enhancement of Photocurrent Generation on a Molecular Monolayer System. *J. Phys. Chem. C* **2012**, *116*, 20806−20811.

(16) Choi, H.; Chen, W. T.; Kamat, P. V. Know Thy Nano Neighbor. Plasmonic versus Electron Charging Effects of Metal Nanoparticles in Dye-Sensitized Solar Cells. *ACS Nano* **2012**, *6*, 4418−4427.

(17) Ueno, K.; Juodkazis, S.; Shibuya, T.; Yokota, Y.; Mizeikis, V.; Sasaki, K.; Misawa, H. Nanoparticle Plasmon-Assisted Two-Photon Polymerization Induced by Incoherent Excitation Source. *J. Am. Chem. Soc.* **2008**, *130*, 6928−6929.

(18) Wang, D. H.; Kim, D. Y.; Choi, K. W.; Seo, J. H.; Im, S. H.; Park, J. H.; Park, O. O.; Heeger, A. J. Enhancement of Donor−Acceptor Polymer Bulk Heterojunction Solar Cell Power Conversion Efficiencies by Addition of Au Nanoparticles. *Angew. Chem., Int. Ed.* **2011**, *50*, 5519−5523.

(19) Manai, I.; Horchani, R.; Lignier, H.; Pillet, P.; Comparat, D.; Fioretti, A.; Allegrini, M. Rovibrational Cooling of Molecules by Optical Pumping. *Phys. Rev. Lett.* **2012**, *109*, 183001.

(20) Shuman, E. S.; Barry, J. F.; DeMille, D. Laser Cooling of a Diatomic Molecule. *Nature* **2010**, *467*, 820−823.

(21) Mansuripur, M. Optical Manipulation: Momentum Exchange Effect. *Nat. Photonics* **2013**, *7*, 765−766.

(22) Ikeda, K.; Takase, M.; Hayazawa, N.; Kawata, S.; Murakoshi, K.; Uosaki, K. Plasmonically Nano-Confined Light Probing Invisible

Phonon Modes in Defect-Free Graphene. *J. Am. Chem. Soc.* **2013**, *135*, 11489−11492.
(23) Gibbons, W. M.; Shannon, P. J.; Sun, Sh-T.; Swetlin, B. J. Surface-Mediated Alignment of Nematic Liquid Crystals with Polarized Laser Light. *Nature* **1991**, *351*, 49−50.
(24) Ikeda, T.; Tsutsumi, O. Optical Switching and Image Storage by Means of Azobenzene Liquid-Crystal Films. *Science* **1995**, *268*, 1873−1875.
(25) Reuter, M. G.; Sukharev, M.; Seideman, T. Laser Field Alignment of Organic Molecules on Semiconductor Surfaces: Toward Ultrafast Molecular Switches. *Phys. Rev. Lett.* **2008**, *101*, 208303.
(26) Artamonov, M.; Seideman, T. Molecular Focusing and Alignment with Plasmon Fields. *Nano Lett.* **2010**, *10*, 4908−4912.
(27) Kohoutek, J.; Dey, D.; Bonakdar, A.; Gelfand, R.; Sklar, A.; Memis, O. G.; Mohseni, H. Opto-Mechanical Force Mapping of Deep Subwavelength Plasmonic Modes. *Nano Lett.* **2011**, *11*, 3378−3382.
(28) Shoji, T.; Saito, J.; Kitamura, N.; Nagasawa, F.; Murakoshi, K.; Tsuboi, Y. Permanent Fixing or Reversible Trapping and Release of DNA Micropatterns on a Gold Nanostructure Using Continuous-Wave or Femtosecond-Pulsed Near-Infrared Laser Light. *J. Am. Chem. Soc.* **2013**, *135*, 6643−6648.
(29) Ratner, M. A. Introducing Molecular Electronics. *Mater. Today* **2002**, *5*, 20−27.
(30) Chen, F.; Hihath, J.; Huang, Z.; Li, X.; Tao, N. J. Measurement of Single-Molecule Conductance. *Annu. Rev. Phys. Chem.* **2007**, *58*, 535−564.
(31) Jain, P. K.; Huang, W.; El-Sayed, M. A. On the Universal Scaling Behavior of the Distance Decay of Plasmon Coupling in Metal Nanoparticle Pairs: A Plasmon Ruler Equation. *Nano Lett.* **2007**, *7*, 2080−2088.
(32) Su, K.-H.; Wei, Q.-H.; Zhang, X.; Mock, J. J.; Smith, D. R.; Schultz, S. Interparticle Coupling Effects on Plasmon Resonances of Nanogold Particles. *Nano Lett.* **2003**, *3*, 1087−1090.
(33) Knight, M. W.; Sobhani, H.; Nordlander, P.; Halas, N. J. Photodetection with Active Optical Antennas. *Science* **2011**, *332*, 702−704.
(34) Stamenkovic, V. R.; Fowler, B.; Mun, B. S.; Wang, G.; Ross, P. N.; Lucas, C. A.; Markovic, N. M. Improved Oxygen Reduction Activity on $Pt_3Ni(111)$ via Increased Surface Site Availability. *Science* **2007**, *315*, 493−497.
(35) Ulman, A. Formation and Structure of Self-Assembled Monolayers. *Chem. Rev.* **1996**, *96*, 1533−1554.
(36) Bertolini, J. C.; Tardy, B. Vibrational EELS Studies of CO Chemisorption on Clean andCarbided (111), (100) and (110) Nickel Surfaces. *Surf. Sci.* **1981**, *102*, 131−150.
(37) Ikeda, K.; Sato, J.; Fujimoto, N.; Hayazawa, N.; Kawata, S.; Uosaki, K. Plasmonic Enhancement of Raman Scattering on Non-SERS-Active Platinum Substrates. *J. Phys. Chem. C* **2009**, *113*, 11816−11821.
(38) Li, J. F.; Ding, S. Y.; Yan, Z. L.; Bai, M. L.; Anema, J. R.; Wang, X.; Wang, A.; Wu, D. Y.; Ren, B.; Hou, S. M.; et al. Extraordinary Enhancement of Raman Scattering from Pyridine on Single Crystal Au and Pt Electrodes by Shell-Isolated Au Nanoparticles. *J. Am. Chem. Soc.* **2011**, *133*, 15922−15925.
(39) Yano, T.; Verma, P.; Saito, Y.; Ichimura, T.; Kawata, S. Pressure-Assisted Tip-Enhanced Raman Imaging at a Resolution of a Few Nanometers. *Nat. Photonics* **2009**, *3*, 473−477.
(40) Liu, Z.; Ding, S. Y.; Chen, Z. B.; Wang, X.; Tian, J. H.; Anema, J. R.; Zhou, X. S.; Wu, D. Y.; Mao, B. W.; Xu, X.; et al. Revealing the Molecular Structure of Single-Molecule Junctions in Different Conductance States by Fishing-Mode Tip-Enhanced Raman Spectroscopy. *Nat. Commun.* **2011**, *2*, 1−6.
(41) Ikeda, K.; Fujimoto, N.; Uehara, H.; Uosaki, K. Raman Scattering of Aryl Isocyanide Monolayers on Atomically Flat Au(1 1 1) Single Crystal Surfaces Enhanced by Gap-Mode Plasmon Excitation. *Chem. Phys. Lett.* **2008**, *460*, 205−208.
(42) Ikeda, K.; Sato, J.; Uosaki, K. Surface-Enhanced Raman Scattering at Well-Defined Single Crystalline Faces of Platinum-Group Metals Induced by Gap-Mode Plasmon Excitation. *J. Photochem. Photobiol., A* **2011**, *221*, 175−180.
(43) Ikeda, K.; Suzuki, S.; Uosaki, K. Crystal Face Dependent Chemical Effects in Surface Enhanced Raman Scattering at Atomically Defined Gold Facets. *Nano Lett.* **2011**, *11*, 1716−1722.
(44) Ikeda, K.; Suzuki, S.; Uosaki, K. Enhancement of SERS Background through Charge Transfer Resonances on Single Crystal Gold Surfaces of Various Orientations. *J. Am. Chem. Soc.* **2013**, *135*, 17387−17392.
(45) Nordlander, P.; Prodan, E. Plasmon Hybridization in Nanoparticles near Metallic Surfaces. *Nano Lett.* **2004**, *4*, 2209−2213.
(46) Aravind, P. K.; Metiu, H. Use of a Perfectly Conducting Sphere To Excite the Plasmon of a Flat Surface. 1. Calculation of the Local Field with Applications to Surface-Enhanced Spectroscopy. *J. Phys. Chem.* **1982**, *86*, 5076−5084.
(47) Aravind, P. K.; Metiu, H. The Effects of the Interaction between Resonances in the Electromagnetic Response of a Sphere-Plane Structure; Applications to Surface Enhanced Spectroscopy. *Surf. Sci.* **1983**, *124*, 506−528.
(48) Clavilier, J.; Faure, R.; Guinet, G.; Durand, R. Preparation of Monocrystalline Pt Microelectrodes and Electrochemical Study of the Plane Surfaces Cut in the Direction of the (111) and (110) Planes. *J. Electroanal. Chem.* **1980**, *107*, 205−209.
(49) Kim, K.; Choi, J. Y.; Shin, K. S. Enhanced Raman Scattering in Gaps Formed by Planar Au and Au/Ag Alloy Nanoparticles. *J. Phys. Chem. C* **2013**, *117*, 11421−11427.
(50) Wind, M. M.; Vlieger, J.; Bedeaux, D. The Polarizability of a Truncated Sphere on a Substrate II. *Physica A* **1987**, *141*, 33−57.
(51) Okamoto, T.; Yamaguchi, I. Optical Absorption Study of the Surface Plasmon Resonance in Gold Nanoparticles Immobilized onto a Gold Substrate by Self-Assembly Technique. *J. Phys. Chem. B* **2003**, *107*, 10321−10324.
(52) Otto, A.; Mrozek, I.; Grabhorn, H.; Akemann, W. Surface-Enhanced Raman Scattering. *J. Phys.: Condens. Matter* **1992**, *4*, 1143−1212.
(53) Moskovits, M. Surface-Enhanced Spectroscopy. *Rev. Mod. Phys.* **1985**, *57*, 783−826.
(54) Pettinger, B. Light Scattering by Adsorbates at Ag Particles: Quantum-Mechanical Approach for Energy Transfer Induced Interfacial Optical Processes Involving Surface Plasmons, Multipoles, and Electron-Hole Pairs. *J. Chem. Phys.* **1986**, *85*, 7442−7451.
(55) García-Vidal, F. J.; Pendry, J. B. Collective Theory for Surface Enhanced Raman Scattering. *Phys. Rev. Lett.* **1996**, *77*, 1163−1166.
(56) Lombardi, J. R.; Birke, R. L.; Lu, T.; Xu, J. Charge-Transfer Theory of Surface Enhanced Raman Spectroscopy: Herzberg-Teller Contributions. *J. Chem. Phys.* **1986**, *84*, 4174−4180.
(57) Kim, N. H.; Kim, K. Adsorption Characteristics of Arylisocyanide on Au and Pt Electrode Surfaces: Surface-Enhanced Raman Scattering Study. *J. Phys. Chem. B* **2006**, *110*, 1837−1842.
(58) Gruenhaum, S. M.; Henney, M. H.; Kumar, S.; Zou, S. Surface-Enhanced Raman Spectroscopic Study of 1,4-Phenylene Diisocyanide Adsorbed on Gold and Platinum-Group Transition Metal Electrodes. *J. Phys. Chem. B* **2006**, *110*, 4782−4792.
(59) Lombardi, J. R.; Birke, R. L. Excitation Profiles and the Continuum in SERS: Identification of Fano Line Shapes. *J. Phys. Chem. C* **2010**, *114*, 7812−7815.
(60) Hammer, B.; Nørskov, J. K. Theoretical Surface Science and Catalysis - Calculations and Concepts. *Adv. Catal.* **2000**, *45*, 71−129.
(61) Radilla, J.; Boronat, M.; Corma, A.; Illas, F. Monitoring the Interaction of Adsorbates on Metal Surfaces by Surface Site Engineering: the Case of Ethoxy on Cu, Pd, Ag and Au Regular and Stepped Surfaces. *Phys. Chem. Chem. Phys.* **2010**, *12*, 6492−6498.
(62) Ito, M.; Noguchi, H.; Ikeda, K.; Uosaki, K. Substrate Dependent Structure of Adsorbed Aryl Isocyanides Studied by Sum Frequency Generation (SFG) Spectroscopy. *Phys. Chem. Chem. Phys.* **2010**, *12*, 3156−3163.